Nano Energy 45 (2018) 398–406

Contents lists available at ScienceDirect

Nano Energy

journal homepage: www.elsevier.com/locate/nanoen

Full paper

Strongly enhanced dielectric and energy storage properties in lead-free perovskite titanate thin films by alloying

Seungho Cho[a,b,*,1], Chao Yun[b,1], Yoon Seo Kim[a,1], Han Wang[c], Jie Jian[c], Wenrui Zhang[d], Jijie Huang[c], Xuejing Wang[c], Haiyan Wang[c,e], Judith L. MacManus-Driscoll[b,**]

[a] School of Materials Science and Engineering, Ulsan National Institute of Science and Technology (UNIST), Ulsan 44919, Republic of Korea
[b] Department of Materials Science and Metallurgy, University of Cambridge, 27 Charles Babbage Road, Cambridge CB3 0FS, United Kingdom
[c] School of Materials Engineering, Purdue University, West Lafayette, IN 47907, United States
[d] Brookhaven National Laboratory, Shirley, NY 11967, United States
[e] School of Electrical and Computer Engineering, Purdue University, West Lafayette, IN 47907, United States

ARTICLE INFO

Keywords:
Crystallinity
Solid solution
Energy storage
Lead-free perovskite
Dielectric property

ABSTRACT

Lead-free perovskite oxide thin films prepared by alloying of titanates and materials with lower melting points are shown to have enhanced ferroelectric and dielectric properties. $BaTiO_3$ (or $SrTiO_3$) with 25% addition of $BiFeO_3$ has much improved crystalline perfection because of the lower melting point of the $BiFeO_3$ giving enhanced growth kinetics. The maximum dielectric peak temperature of $BaTiO_3$ is increased by ~ 200 °C and leakage currents are reduced by up to a factor of ~ 100. The loss tangent reduces up to 300 °C, with a factor of > 14 reduction at room temperature. The dielectric breakdown strength is higher by a factor of ~ 3 (> 2200 kV cm^{-1}) and from room temperature up to 500 °C the dielectric constant is > 1000. Also, a low variation of dielectric constant of ~ 9% from room temperature to 330 °C is obtained, compared to ~ 110% for $BaTiO_3$. The maximum polarization (P_{max}) is double that of $BaTiO_3$, at 125.3 μC cm^{-2}. The film has high energy storage densities of > 52 J cm^{-3} at 2050 kV cm^{-1}, matching Pb-based ferroelectric films. The strongly improved performance is important for applications in energy storage and in high temperature (up to 300 °C) capacitors as well as wider application in other electronic and energy technologies.

1. Introduction

Ferroelectric materials including normal ferroelectrics, relaxor ferroelectrics and antiferroelectrics exhibit the effect of spontaneous electric polarization which can be reversed by electric field application [1,2]. Because of their electric polarization behaviors and unique dielectric properties, they have been widely investigated for various applications such as capacitors, energy harvesting and storage, high-power electronic transducers, electrocaloric cooling/heating devices, microwave electronics and non-volatile memories [3–7]. For such applications of dielectric or ferroelectric materials, low leakage current and high breakdown strength in addition to high electric polarization and dielectric constant are required. While epitaxial ferroelectric films have higher densities and lower defect concentrations than bulk and properties can be improved by epitaxial constraints [8–10], making them capable of withstanding high electric fields (typically, one order of magnitude higher breakdown strength than bulk ceramics) and possessing exceptionally large volume specific energy storage density [11–13], they are still far from ideal. In particular, oxide thin films have crystallographic defects which negatively impact breakdown strength [14]. The continuing drive towards miniaturization of electronic circuits and devices is motivating the development of new 'thin film' materials [15].

The family of perovskites with the general formula ABO_3 (A: cation at the vertices of the cube, B: cation at the body center) is an important class of ferroelectric materials. Industry-standard ferroelectric perovskites contain lead, which is toxic and environmentally unfriendly because lead-free materials normally exhibited inferior ferroelectric properties to those of the lead-based materials [16]. However, in consideration of the growing demand for green materials with minimized impacts on health and environment, lead-free compositions are urgently required [17,18].

Solid solutions yield the opportunity to create improved [19–21], unexpected or superior properties beyond averaging of their end

* Corresponding author at: School of Materials Science and Engineering, Ulsan National Institute of Science and Technology (UNIST), Ulsan 44919, Republic of Korea.
** Corresponding author.
E-mail addresses: scho@unist.ac.kr (S. Cho), jld35@cam.ac.uk (J.L. MacManus-Driscoll).
[1] S.C., C.Y. and Y.S.K. contributed equally to this work.

https://doi.org/10.1016/j.nanoen.2018.01.003
Received 27 September 2017; Received in revised form 1 January 2018; Accepted 1 January 2018
Available online 03 January 2018

member properties [22,23]. Careful choice of end members and their compositions is required. Although ferroelectric epitaxial solid solution thin films have been reported so far [24–28], the idea of enhancing ferroelectric and dielectric properties in Pb-free ferroelectrics films by selecting the right chemistry for defect reduction *at the same time as* enhancement of the temperature of the dielectric maximum has not been considered to date. In this study, we propose and demonstrate a way to do this. The parent materials chosen are standard $BaTiO_3$ (BTO) or $SrTiO_3$ (STO) with $BiFeO_3$ (BFO) additions. On their own these compositions have the following salient and detrimental points:

BTO and STO are well-investigated oxide ferroelectrics with distinct structural and electrical properties. The materials are easy to grow in thin films form. Epitaxial quality, crystallinity and defect density of films have a significant influence on electrical properties of the films with many oxide ferroelectric films having far too high defect concentrations [29], especially compared to perfect single crystals. A key reason for this is the poor kinetics of growth of oxide films [30], i.e. they are grown far below their melting points. This makes the film has many defects as well as it making strain-relief by misfit dislocations difficult, consequently leading to a wide range of other more deleterious defects [31]. Other problems of BTO and STO are their low ferroelectric Curie temperatures (T_cs) which are too low to be practical for many applications [4,32]. For BTO, T_c is ~ 130 °C, and STO is ferroelectric only at cryogenic temperatures [33,34]. Indeed, it is paraelectric at room temperature. BFO has a high Curie temperature, T_c: ~ 850 °C) [35,36]. However, it is very prone to defects and its high leakage current value limits its use in electronic devices [37]. Its rhombohedral structure means it is hard to grow on the standard single crystal substrate, STO, to give ideal ferroelectric properties [38].

For the following reasons, we propose that by combining BTO (or STO) with BFO there may be benefits of both enhanced maximum dielectric peak temperature of the BTO (or STO) *and* reduced defects concentrations:

- Mixing of the higher T_c BFO phase with the lower T_c titanate gives an enhancement of the temperature of the dielectric permittivity maximum [39].
- Bi-based compound additions to ceramics enhance growth kinetics [40]. In particular, there is a low melting eutectic between Bi_2O_3 and TiO_2 with the possibility of quasi-equilibrium effects which can reduce this temperature further [41]. Hence, there should be a strong chance for defect reduction in BTO and STO in this work. The key question to answer is what level of BFO addition gives this beneficial effect *without* it being too high that the inherent defects associated with BFO will degrade the ferroelectric properties.

In this study, the different thin film compositions were deposited under the same conditions on single crystalline STO substrates. STO is the most established single crystalline substrate for film growth, and is the most promising oxide buffer on Si, the key end-goal substrate for the oxide electronics field [42,43]. We explored a range of compositions across the BTO (or STO)-BFO compositional line. We denote pure and solid solution films of BFO-BTO with the molar percentage of 100:0 and 75:25 as BFO100 and BFO75-BTO25 hereafter, respectively. We show a linear relation of unit cell volume of the BTO (or STO) films with fraction of BFO added to them, indicative of a clean solid solution across the whole compositional range, which is further supported by transmission electron microscopy. Most importantly, we show for the first time how to strongly improve the ferroelectric performance of titanate films while also increasing their maximum dielectric peak temperatures. We find BFO25-BTO75 and BFO25-STO75 to be the optimum film compositions. These compositions have the highest crystallinities, macroscopic ferroelectric properties and dielectric properties and they are strongly improved compared to BTO100 and STO100, respectively. The BFO25-BTO75 film has a high dielectric constant (> 1000) from room temperature to 500 °C and shows a high dielectric constant stability, $\frac{\Delta C}{C_{RT}}$ (from room temperature to 330 °C) of ~ 9%. Also, the leakage current is lowest for this composition and the breakdown strength highest (> 2200 kV cm^{-1}). The high breakdown strength and maximum polarization (P_{max}) of the BFO25-BTO75 film and the BFO25-STO75 film gives electric energy densities (W) of: 52.2 J cm^{-3} and 31.8 J cm^{-3}, respectively, as high as the highest reported values for lead-based materials [44,45]. Hence, there are excellent prospects for the solid solution composition films of this work in energy storage applications. In addition, high temperature capacitor applications, e.g. in electric vehicles, avionics and downhole electronics, could strongly benefit from the high and relatively flat temperature dependent-dielectric constants and low losses demonstrated here.

2. Material and methods

Film fabrication: $SrRuO_3$ (SRO)-buffered $SrTiO_3$ (STO) (001) substrates (areas: 0.5 × 0.5 cm^2) were used. SRO layers (nominal thickness of 38 nm) were grown as bottom electrodes on STO (001) substrate by pulsed laser deposition (PLD) with a KrF laser (λ = 248 nm) with fluences of 2.25 J cm^{-2} and repetition rates of 1 Hz. The growth rates of the SRO layers are 0.05 nm s^{-1}. The heater temperature of 715 °C and the oxygen pressure of 0.2 mbar were maintained during deposition. The SRO films was post-annealed at 450 °C for 1 h under 400 mbar O_2 and cooled at a rate of 15 °C min^{-1}. $BiFeO_3$ (BFO)-$BaTiO_3$ (BTO) targets and BFO-STO targets were prepared by thoroughly mixing stoichiometric amounts of Bi_2O_3, Fe_2O_3, BTO and STO with bismuth excess for preventing bismuth deficiency, followed by sintering at 800 °C. Films were grown on the SRO-buffered STO (001) substrates by PLD with fluences of 2.25 J cm^{-2} and repetition rates of 1 Hz. The film growth rates of 0.14 nm s^{-1} were kept the same for all the sample by controlling distances from the targets and substrates. During deposition, the heater temperature was 715 °C and the oxygen pressure was 0.2 mbar. Pt electrodes were deposited by DC-magnetron sputtering onto the film surface with shadow masks for electrical measurements.

Charaterizations: The phase and the crystalline quality of the thin films were investigated by ω-2θ and asymmetric X-ray diffraction (XRD) on a PANalytical Empyrean high resolution X-ray diffractometer. Reciprocal space maps (RSMs) were collected about the (103) of STO substrates. ω-2θ diffraction peaks and RSM peaks were used to calculate lattice parameters of the films. For investigating in-plane orientation, phi (φ) scans were obtained by 360° in-plane sample rotation around (111) peaks of the films and substrates. Transmission electron microscopy (TEM) was performed using a FEI Tecnai G2 F20 microscope, operated at 200 kV. We measured leakage currents using a two-probe station and a Keithley 2440 source-meter. A Radiant 100 Precision ferroelectric tester was used to measure the room temperature polarization versus electric field (P-E) hysteresis loops. To measure dielectric constants with temperature variation, we used a hot plate and an HP 4294A Precision Impedance Analyser. The dielectric constant was measured with frequency, and its dependence on temperature extracted at 1, 5, 25 and 120 kHz with a 50 mV field.

3. Results and discussion

BFO, BTO, STO and their mixture films were deposited on conducting $SrRuO_3$ (SRO)-buffered STO substrates by pulsed laser deposition (PLD) with the same growth conditions except target compositions. The SRO buffer layers are used as bottom electrodes for electric measurements [46]. The nominal thicknesses of the films and SRO buffer layers are ~ 180 nm and ~ 38 nm. The estimated compositions of the mixture films are measured and provided in the Supporting information (Table S1).

The room temperature ferroelectric properties of the films across the solid solution series were characterized by the polarization hysteresis method. The BFO100, BFO75-BTO25 and BFO50-BTO50 films showed

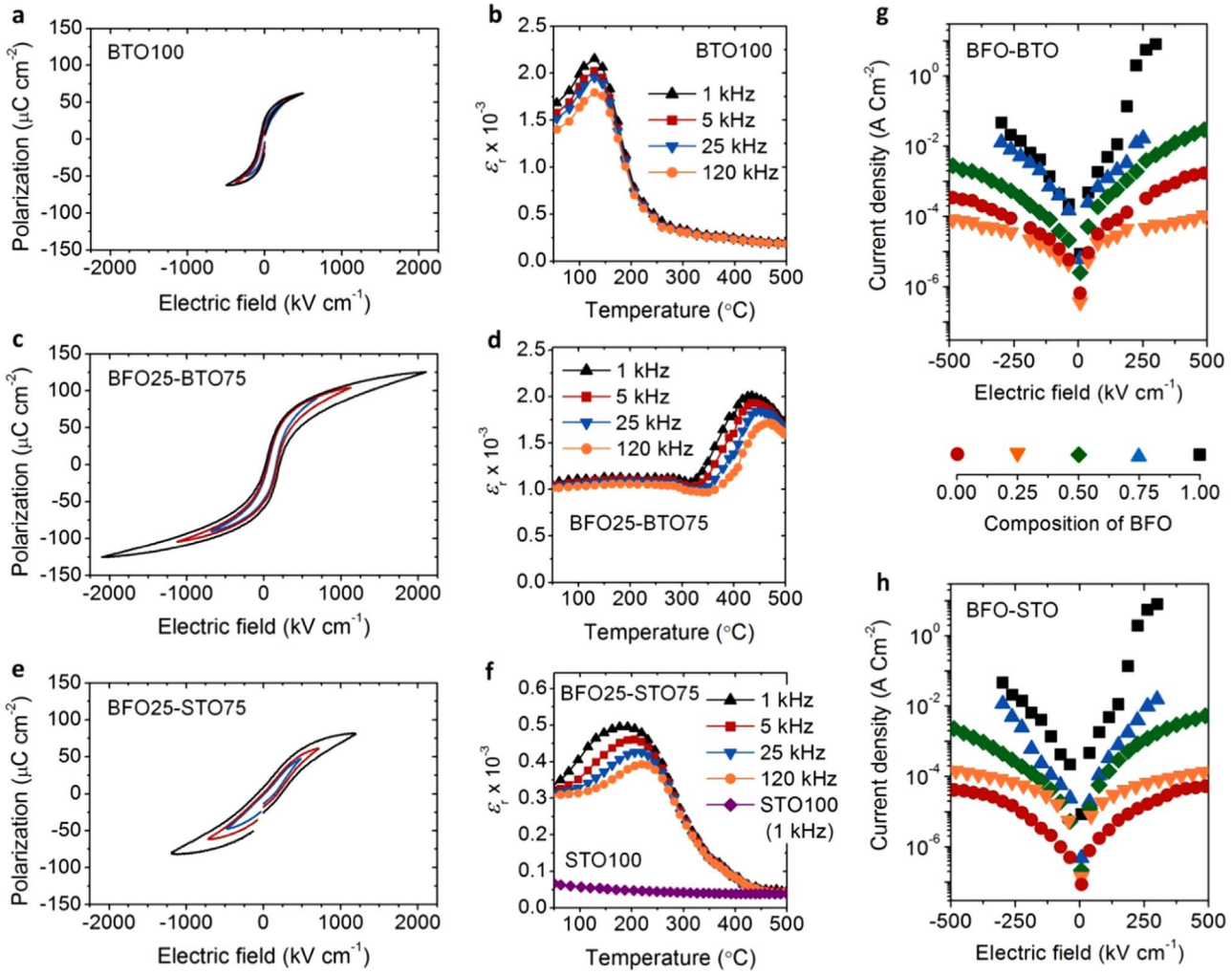

Fig. 1. Polarization versus electric field loops for (a) $BaTiO_3$ (BTO)100 film, (c) $BiFeO_3$ (BFO)25-BTO75 film and (e) BFO25-$SrTiO_3$ (STO)75 film. Temperature dependence of relative dielectric constants of (b) BTO100 film, (d) BFO25-BTO75 film and (f) BFO25-STO75 film and STO100 film at different frequencies. Leakage current density as a function of electric field measured at room temperature for (g) BFO, BTO and their solid solution films and (h) BFO, STO and their solid solution films.

leaky polarization versus electric field (*P-E*) curves (Fig. S1 in the Supporting information). This is not surprising considering the high BFO fractions. On the other hand, the BTO100 film exhibits a macroscopic ferroelectric property. Fig. 1a shows *P-E* hysteresis loops for the BTO100 film. The maximum polarization (P_{max}), saturation polarization (P_s), remanent polarization (P_r) and coercive field (E_c) values for the BTO100 film are 62.4 μC cm^{-2}, 51.1 μC cm^{-2}, 31.2 μC cm^{-2}, and 42 kV cm^{-1}, respectively, with the applied electric field range of ± 500 kV cm^{-1}, which are comparable to those of epitaxial BTO films in the literatures [47–50]. Fig. 1b shows the dielectric constants as a function of temperature for the BTO100 film. We observe a peak at 127 °C, coinciding with the T_c of BTO. There is no shift in this peak position with frequency, indicating a displacive, rather than diffuse, phase transition [51].

Fig. 1c shows *P-E* hysteresis loops for the BFO25-BTO75 film, which was found to give the lowest leakage current across the solid solution series (Fig. 1g). The P_{max}, P_s, P_r, and E_c values for the BFO25-BTO75 film are 125.3 μC cm^{-2}, 98.2 μC cm^{-2}, 36.6 μC cm^{-2}, and 75 kV cm^{-1}, respectively, at an applied electric field range of ± 2100 kV cm^{-1}. The P_{max} and P_s values are 101% and 92% higher than the highest measured values for the BTO100 film (62.4 μC cm^{-2} and 51.1 μC cm^{-2}, Fig. 1a) deposited under the same deposition conditions, respectively.

Fig. 1d shows the dielectric constants as a function of temperature for the BFO25-BTO75 film. The film has high dielectric constants (> 1000) from room temperature up to 500 °C and shows a typical behavior of relaxors, i.e. a smeared maxima of dielectric permittivity with the temperature of the maximum shifting toward higher temperatures with increasing measurement frequency [52]. The dielectric constant stability of the film against temperature is defined as

$$\frac{\Delta C}{C_{RT}} = \frac{\varepsilon_{max} - \varepsilon_{min}}{\varepsilon_{RT}} \times 100\% \quad (1)$$

where ε_{max}, ε_{min}, and ε_{RT} are respectively the maximum, minimum and room temperature dielectric constants [53]. The optimum BFO25-BTO75 film shows a very high dielectric constant stability, $\frac{\Delta C}{C_{RT}}$ (from room temperature to 330 °C) of ~ 9% (Table S2 in the Supporting information). $\frac{\Delta C}{C_{RT}}$ of most conventional X7R (up to 125 °C) and X8R (up to 150 °C) capacitors are ~ 15%. Also, this film composition has a dielectric constant higher than 1000 with high stability at temperatures up to 330 °C, which is also a very promising feature for high temperature capacitor applications.

We now focus on the STO-BFO compositions. We see that the STO100 film shows a paraelectric characteristic at room temperature, as expected. Consistent with the comparator BTO composition with high BFO fraction, the BFO75-STO25 and BFO50-STO50 films exhibit leaky *P-E* curves (Fig. S2 in the Supporting information). On the other hand, the BFO25-STO75 film exhibits macroscopic ferroelectric properties (Fig. 1e). The P_{max}, P_s, P_r, and E_c values for the BFO25-STO75 film are 81.7 μC cm^{-2}, 71.4 μC cm^{-2}, 16.5 μC cm^{-2}, and 139 kV cm^{-1},

respectively, within the applied electric field range of ± 1200 kV cm^{-1}.

The P_{max} and P_s values of the BFO25-BTO75 (Fig. 1c) and BFO25-STO75 (Fig. 1e) films are comparable to those of lead-based thin films in the literatures [54–57]. Again, consistent with the comparator BTO composition with high BFO fraction the temperature dependence of the dielectric constant for the BFO25-STO75 film (Fig. 1f) show a typical relaxor behavior with dielectric constants higher than for the STO100 film from room temperature to 500 ºC.

For any dielectric application of the thin films, leakage currents need to be minimized [58]. Figs. 1g and 1h show the leakage current densities of the BFO100, BTO100, STO100 and their solid solution films at room temperature as a function of applied electric fields. At an electric field of − 200 kV cm^{-1} the BTO100 and STO100 films show leakage currents more than two orders of magnitude lower than that of the BFO100 film (Figs. 1g and 1h). Going across the solid solution series, there is a general trend that the more BFO in the film, the higher the leakage. This is expected since without extreme care of growth optimization for BFO, it is a very leaky material [59]. Fe ions can act as trap centres, and oxygen vacancies formed during growth cause a portion of the Fe^{3+} ions to become Fe^{2+} [60]. Also, Bi non-stoichiometry is prevalent and leads to a range of defects which increase leakage [8]. The leaky natures of the films with a higher fraction than 50% of BFO are also manifest in leaky *P-E* curves (Figs. S1 and S2 in the Supporting information).

Interestingly, the BFO25-BTO75 film exhibits lower leakage current densities than BTO100. We hypothesize that the enhanced crystalline perfection of BTO induced by the low level BFO addition outweighs the inherent leaky nature of the BFO. Evidence to support this hypothesis is shown later. Up to ~ 300 °C in the BFO25-BTO75 case and to ~ 100 °C in the BFO25-STO75 case, the 25% BFO-doped titanate films exhibit lower loss tangent values than the BTO100 films (Fig. 2).

Detailed understanding of the nature of the improved ferroelectric and dielectric properties of the films was obtained from a range of X-ray diffraction (XRD) measurements as well as transmission electron microscopy (TEM). The crystalline natures of the film were investigated using four-circle XRD. Fig. 3 shows XRD ω-2θ scans for the BFO, BTO, STO and their mixture films (see also Fig. S3 in the Supporting information for XRD ω-2θ scans with wider 2θ ranges) indicating that the films were well crystallized and highly crystallographically oriented (film growth directions: [001]). Interestingly, double peaks appeared in addition to the SRO and STO substrate peaks in the BTO100 and BFO100 cases as well as in the BTO-BFO mixtures (Fig. 3a). For the mixed BTO-BFO PLD targets, the possible reasons for the double peaks are the coexistence of relaxed and strained phases [61,62], phase separation of the different metal oxides [63–65], and twinning [66]. This issue will be discussed later in detail. On the other hand, the double peak character of BFO disappears when it is mixed with STO (i.e. the BFO-STO system, Fig. 3b). As the concentration of STO increases, the (002) peaks are sharper and have higher intensities and the positions of the (00*l*) reflections are gradually shifted to higher 2θ (Fig. 3b), indicating reduction of the out-of-plane lattice constants [23].

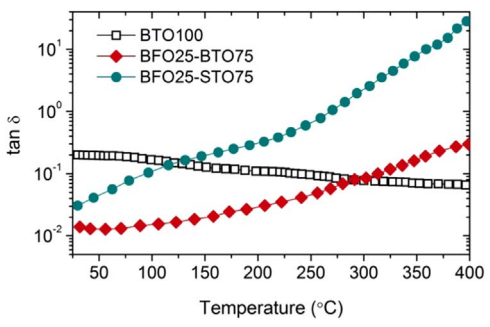

Fig. 2. Temperature dependence of dielectric loss tangent at 25 kHz for the $BaTiO_3$ (BTO) 100, $BiFeO_3$ (BFO)25-BTO75 and BFO25- $SrTiO_3$ (STO)75 films.

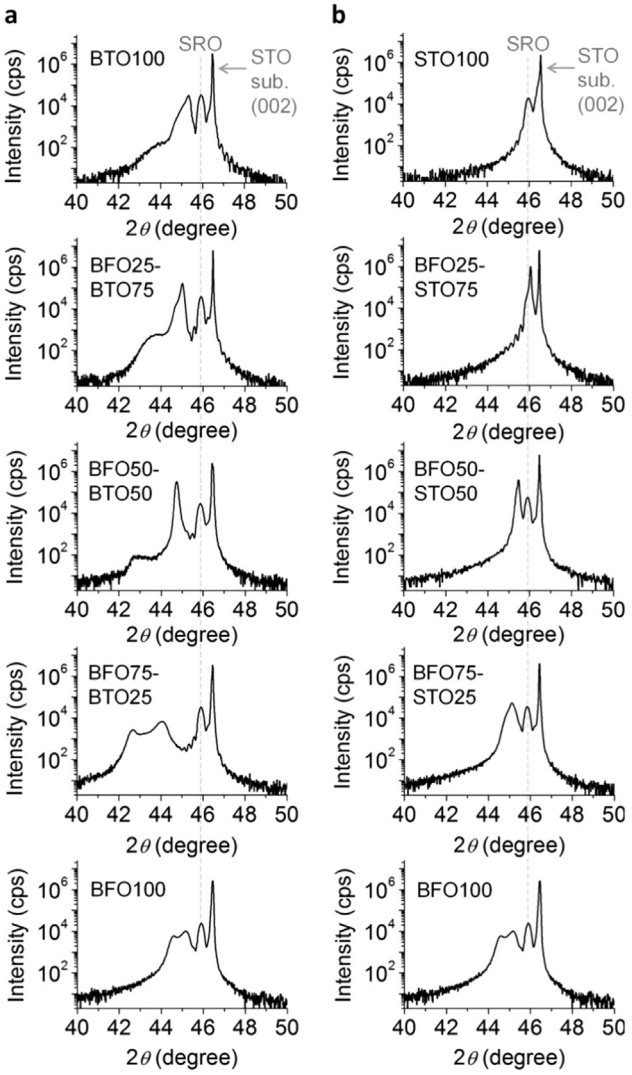

Fig. 3. X-ray diffraction ω-2θ scans of (a) $BaTiO_3$ (BTO), $BiFeO_3$ (BFO) and their mixture films and (b) $SrTiO_3$ (STO), BFO and their mixture films.

As mentioned above, in the cases of the films from the mixed metal oxide PLD targets, the possibilities for phase separations of different metal oxides cannot be ruled out at this point. In this context, Lorenz et al. claimed BFO-BTO nanocomposite film formation based on surface morphology observation by atomic force microscopy (AFM) [67]. However, grains can be observed on surfaces of even one phase plain epitaxial film [68–70]. Thus, we made cross-sectional TEM observations on our mixture films deposited using the mixed metal oxide PLD targets to clarify this issue. Figs. 4a and 4b show representative cross-sectional high-angle annular dark-field (HAADF) scanning transmission electron microscope (STEM) images of the BFO25-BTO75 and BFO75-STO25 films on SRO-buffered STO substrates, respectively. The HAADF-STEM images indicate high uniformity of the composition without phase separation of the different metal oxides [71]. Large range observations of the different composition films also show no phase separation. Therefore, the mixture films are solid solution films.

High-resolution cross-sectional STEM images (Figs. 4c and 4d), selected-area electron diffraction (SAED) patterns along the [010] zone axis (Figs. 4e and 4f) and φ-scans (Fig. S4 in the Supporting information) for the solid solution films on the SRO-buffered STO substrates indicate cube-on-cube epitaxy of the films on the SRO-buffered STO (001) substrates. The epitaxial relationships between the solid solution films, SRO and STO substrate are solid solution [001] // SRO[001] // STO[001], solid solution[100] // SRO[100] // STO[100] and solid

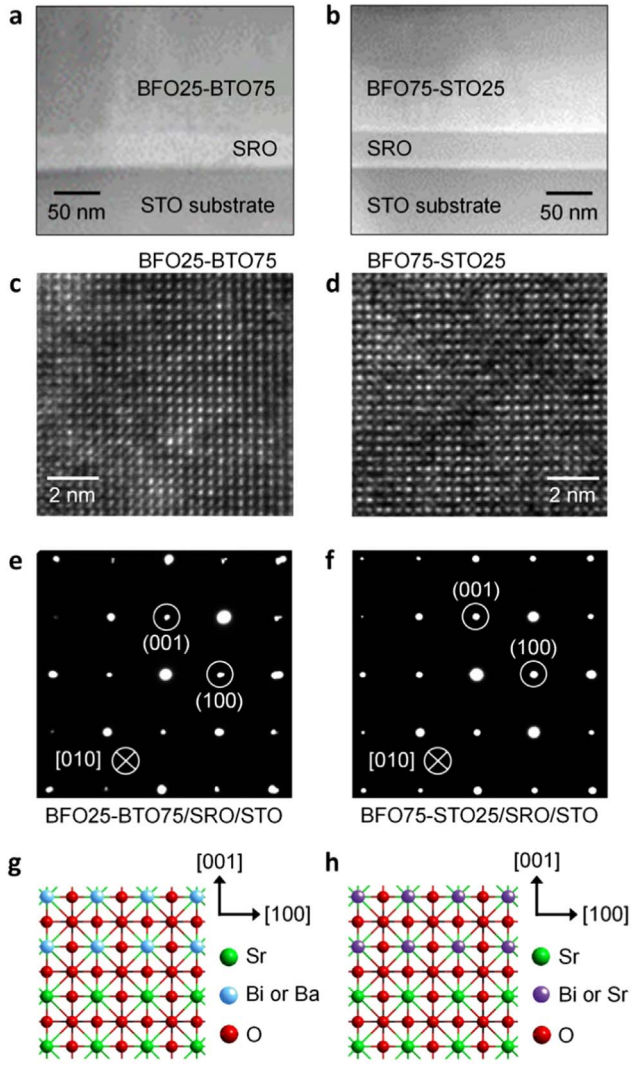

Fig. 4. (a and b) Low magnification cross-sectional high-angle annular dark-field scanning transmission electron microscope (HAADF-STEM) images of $BiFeO_3$ (BFO)25-$BaTiO_3$ (BTO)75 film and BFO75-$SrTiO_3$ (STO)25 film on $SrRuO_3$ (SRO)-buffered STO substrates, respectively. (c and d) High resolution cross-sectional transmission electron microscope images of the films. (e and f) Selected-area electron diffraction (SAED) patterns of the solid solution films, SRO buffer layers and STO substrates along the [010] zone axes. (g and h) Crystallographic models around interfaces between the solid solution films and SRO buffer layers.

solution[110] // SRO[110] // STO[110]. Figs. 4g and 4h show crystallographic models of interfaces between BFO-BTO and BFO-STO solid solution films and SRO buffer layers, respectively, based on the structural characterization results.

To more deeply investigate the uniformity and perfection of the crystalline structures both in-plane and out-of-plane, we obtained XRD reciprocal space maps (RSMs, Figs. 5a and 5b) around the (103) asymmetric peaks. The SRO(103) and film (103) peaks were observed in the lower q_z regions than the high intensity (103) peak of the STO substrate. The q_x positions for SRO(103) peak are, within error range, equal to those of the (103) peaks for the STO substrates, which indicates the SRO buffer layers are fully strained along the in-plane directions. As mentioned briefly for the ω-2θ scans (Fig. 3), the BFO, BTO and the solid solution films have double XRD peaks. They also have double RSM peaks (Fig. 5a). Hence, apart from the BFO-STO system which is structurally compatible with the STO substrate, each film has a broader and stronger peak in the higher q_z region and a narrower and weaker peak in the lower q_z region. The broader film peaks are not aligned with the SRO/STO peaks along the q_x direction indicating the strain relaxation in-plane. The results show that in the BFO, BTO and solid solution films, there is coexistence of both a fully substrate-strained region of the film and a relaxed region [61,62]. The in-plane and out-of-plane lattice parameters of the film determined from measurements of the c parameters from ω-2θ scans (Fig. 3), and by calculating the a parameters based on the centres of the peaks of the main broad film RSM peaks, are shown in Fig. 5b. The lattice parameters are provided in Table S3 of the Supporting information. The unit cell volumes of the BTO (STO) systems decrease (increase) with BFO incorporation, as expected (Fig. 5c). The excellent linearity (obeying Vegard's law) of the plot linking the bulk titanate lattice parameters to the BFO lattice parameters proves the perfect mixing of the different perovskite materials in the films.

Since in our 180 nm thick films, the relaxed region with a broader spread of lattice parameters is the predominant fraction of the film, the structural nature of this region will likely determine the overall ferroelectric properties. The question is how defective, in this majority fraction of the film, one film composition is relative to another and how this relates to the properties. Assessment both of the RSM peak widths and rocking curve widths gives a way to assess the film perfection. The q_x widths (Δq_x) of the film peaks in the RSMs gives a measure of the spread of lattice parameters in each film, a narrower spread indicating better overall crystalline perfection. Both the BFO25-BTO75 and BFO25-STO75 films have significantly lower Δq_x values (as indicated on the plot) than the parent BTO and STO films, consistent with enhanced film growth kinetics with addition of the BFO with the lower melting point (Figs. 5d, 5e, 5f and 5g).

Rocking curve widths ($\Delta\omega$) are also a measure of film perfection since they show how the crystalline grains tilt out of the plane of the film. Figs. 6a and 6b show that the films with higher electrical breakdown strength generally have lower $\Delta\omega$ values. Figure S5 shows the actual rocking curves of the (002) peaks from which the data in Figs. 6a and 6b is drawn. We also see that the films with higher electrical breakdown strength also have lower q_x widths (Figs. 6c and 6d) in line with the $\Delta\omega$ data (Figs. 6a and 6b). Hence, crystalline perfection in terms both of narrowness of lattice parameters *and* better crystalline alignment are both critical to achieving higher electrical breakdown strength.

Enhanced dielectric breakdown strength (Fig. 6), lower leakage current (Figs. 1g and 1h), higher overall P_{max} (Figs. 1c and 1e), all derive from the enhanced crystalline perfection as quantified by the lower Δq_x and $\Delta\omega$ values of the titanate films through addition of BFO, which we attribute enhancement of growth kinetics [41], which in turn leads to lower defect concentrations. The additional key benefit of BFO addition is the increase of the maximum dielectric peak temperatures of the BTO and STO phases, to ~ 450 °C and ~ 200 °C, respectively, making the materials suitable for higher temperature applications.

Apart from the high temperature capacitor applications derived from flat and high dielectric constant from room temperature to 330 °C for the BFO25-BTO75 film, another important application area derived from the enhanced P_{max} and dielectric breakdown strength is in dielectric energy storage. Dielectric capacitors are a promising technology for energy storage devices in high-power applications because of their high-power density, fast charge/discharge time (< 1 μs), low cost, and high thermal and mechanical stability [72–76]. The energy density (W) of a dielectric material is given by

$$W = \int_{P_r}^{P_{max}} EdP \quad (0 \le E \le E_{max}) \tag{2}$$

where E is the applied electric field that causes the variation in electric polarization P, P_r is the remnant polarization, P_{max} is the maximum polarization under the applied electric field and E_{max} is the maximum applied electric field. W of the BTO100 film is 5.6 J cm^{-3}. The high P_{max} and dielectric breakdown strength values of the BFO25-BTO75 film and the BFO25-STO75 film lead to high W values of 52.2 J cm^{-3} and 31.8 J cm^{-3}, respectively. The W of the BFO25-STO75 film is

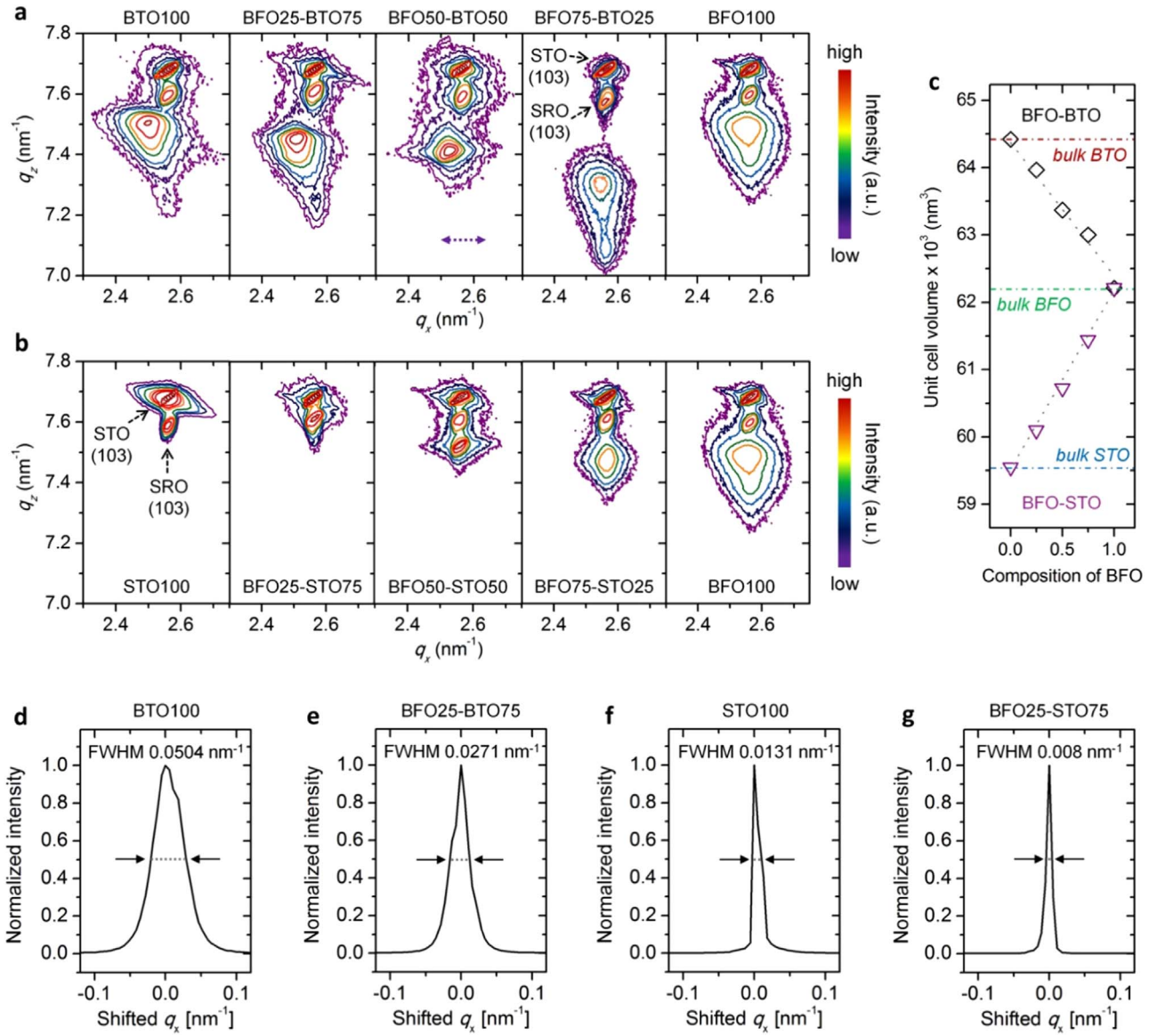

Fig. 5. Reciprocal space maps (RSMs) of (a) $BaTiO_3$ (BTO), $BiFeO_3$ (BFO) and their solid solution films and (b) $SrTiO_3$ (STO), BFO and their solid solution films on $SrRuO_3$ (SRO)-buffered STO substrates around the STO (103) reflections. In the BFO50-BTO50 maps the position of the second peak of the BFO50-BTO50 film is expected to be within the double side arrow based on the ω-2θ scan (Fig. 3). (c) Unit cell volumes of the BFO, BTO, STO, BFO-STO solid solution and BFO-STO solid solution films on the SRO-buffered STO substrates as a function of composition. The volumes were calculated using the in-plane and out-of-plane lattice parameters of the relaxed film peaks in the RSMs, i.e. the broader peaks at higher q_z values. The three horizontal lines indicate the unit cell volumes for bulk BTO, BFO and STO calculated from the Joint Committee on Powder Diffraction Standards (JCPDS) # 89–1428, # 74–2016 and # 35–0734, respectively. Normalized intensities of the (103) peaks of (d) BTO100 film, (e) BFO25-BTO75 film, (f) STO100 film and (g) BFO25-STO75 film determined from the RSMs.

comparable to the highest reported W values from lead-based materials (Fig. 7) [44,45,74–84]. The W value is close to that of $(Bi_{0.5}Na_{0.5})_{0.9118}La_{0.02}Ba_{0.0582}(Ti_{0.97}Zr_{0.03})O_3$ (BNLBTZ) which has a very complex composition [76]. Compared with the BNLBTZ film, our films have simple compositions which means they are easier to process. This work is the first demonstration of what is possible in the mixed titanate-low melting point material system. With further compositional and process optimization, there are strong prospects for yet further performance improvements.

4. Conclusion

In summary, epitaxial lead-free perovskite solid solution thin films of BFO-BTO and BFO-STO were shown to have strongly enhanced dielectric and ferroelectric properties compared to the parent titanate compounds as a result of their much improved crystalline perfection. The improved perfection of both the BTO and STO films can be explained by the enhanced kinetics of film growth in the presence of bismuth compounds with lower melting points. Fig. 8 summarizes the results of this study. The BFO25-BTO75 composition shows the lowest leakage current of any of the compositions, as well as a higher electrical breakdown strength than pure BTO (BTO100). The ferroelectric and dielectric properties correlate directly with the higher crystallinity of the BFO25-BTO75 film. This composition also exhibits high P_{max}, P_s, dielectric constant, dielectric constant stability and electric energy density. The BFO25-STO75 composition shows similar effects with much improved ferrolectric properties which correlate with crystalline perfection. The main difference with BFO25-BTO75 is the lower temperature of the dielectric permittivity maximum (~ 200 °C for BFO25-STO75 *cf.* ~ 450 °C for BFO25-BTO75). P_{max}, the dielectric constant, the thermal stability of dielectric constant and energy storage density of the BFO25-BTO75 film are comparable to the best results of any other lead-free thin films, while also having the advantage of being a much simpler composition. Furthermore, this strategy for enhancing

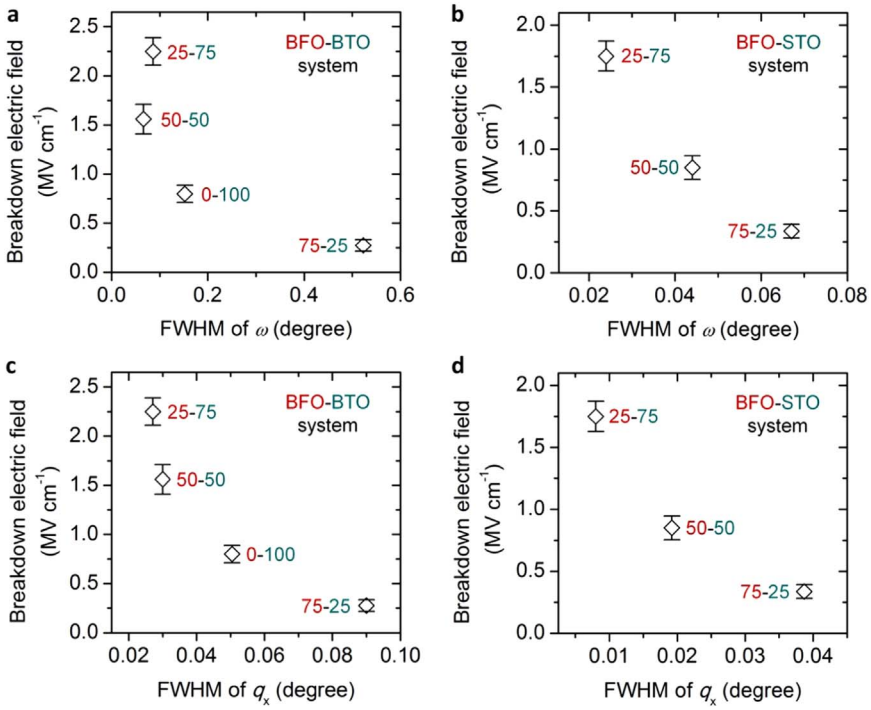

Fig. 6. Breakdown strength of the solid solution films as a function of the full width at half-maximum (FWHM) values of the X-ray diffraction ω-rocking curves for (a) $BiFeO_3$ (BFO)-$BaTiO_3$ (BTO) solid solution system and (b) BFO-$SrTiO_3$ (STO) solid solution system and FWHM q_x values of the (103) peaks on the reciprocal space maps (Figs. 5a and 5b) for (c) BFO-BTO solid solution system and (b) BFO-STO solid solution system. Rocking curve plots from which data in panels a and b are derived are shown in Fig. S5 in the Supporting Information.

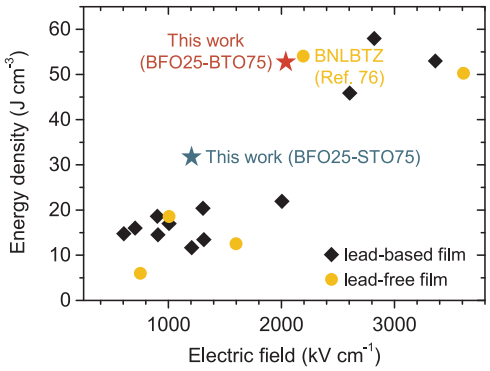

Fig. 7. Comparison of electric energy densities (W) versus electric field for various materials [44,45,74–84].

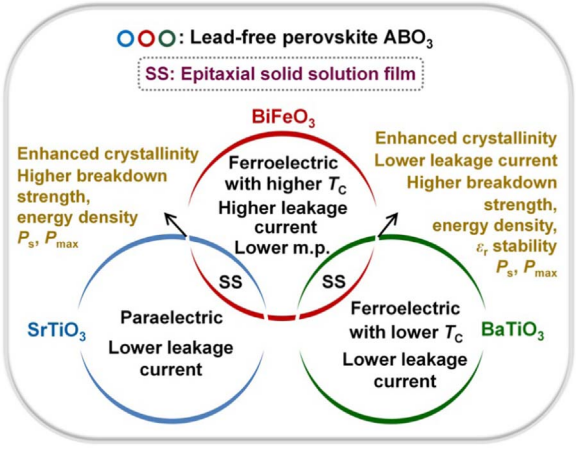

Fig. 8. Diagram describing lead-free perovskite oxides as end members, their solid solution films and their properties.

crystallinity can be extended to other materials than titanates.

Acknowledgements

We acknowledge support from EPSRC grants EP/K035282/1 and EP/N004272/1, the Leverhulme grant RPG-2015-017, and the European Research Council (ERC-2009-AdG 247276 NOVOX). S.C. and Y.S.K. acknowledge the 2017 Research Fund (1.170080.01) of UNIST (Ulsan National Institute of Science & Technology). This work was supported by the National Research Foundation of Korea (NRF) grant funded by the Korea government (MSIP; Ministry of Science, ICT & Future Planning) (No. 2017R1C1B5075626). The TEM work at Purdue University was supported by the U.S. National Science Foundation (DMR-1643911 and DMR-1565822).

Appendix A. Supplementary material

Supplementary data associated with this article can be found in the online version at http://dx.doi.org/10.1016/j.nanoen.2018.01.003

References

[1] W. Känzig, Solid State Physics: Advances in Research and Applications 4 Academic Press Inc, New York, 1957.
[2] M. Lines, A. Glass, Principles and Applications of Ferroelectrics and Related Materials, Clarendon Press, Oxford, 1979.
[3] G.H. Haertling, J. Am. Ceram. Soc. 82 (1999) 797.
[4] S.A. Harrington, J. Zhai, S. Denev, V. Gopalan, H. Wang, Z. Bi, S.A.T. Redfern, S.H. Baek, C.W. Bark, C.B. Eom, Q.X. Jia, M.E. Vickers, J.L. MacManus-Driscoll, Nat. Nanotechnol. 6 (2011) 491.
[5] N. Setter, D. Damjanovic, L. Eng, G. Fox, S. Gevorgian, S. Hong, A. Kingon, H. Kohlstedt, N.Y. Park, G.B. Stephenson, I. Stolitchnov, A.K. Taganstev, D.V. Taylor, T. Yamada, S. Streiffer, J. Appl. Phys. 100 (2006) 051606.
[6] Y.-M. You, W.-Q. Liao, D. Zhao, H.-Y. Ye, Y. Zhang, Q. Zhou, X. Niu, J. Wang, P.-F. Li, D.-W. Fu, Z. Wang, S. Gao, K. Yang, J.-M. Liu, J. Li, Y. Yan, R.-G. Xiong, Science 357 (2017) 306.
[7] J.F. Scott, Science 315 (2007) 954.
[8] J. Wang, J.B. Neaton, H. Zheng, V. Nagarajan, S.B. Ogale, B. Liu, D. Viehland, V. Vaithyanathan, D.G. Schlom, U.V. Waghmare, N.A. Spaldin, K.M. Rabe, M. Wuttig, R. Ramesh, Science 299 (2003) 1719.
[9] K.J. Choi, M. Biegalski, Y.L. Li, A. Sharan, J. Schubert, R. Uecker, P. Reiche, Y.B. Chen, X.Q. Pan, V. Gopalan, L.-Q. Chen, D.G. Schlom, C.B. Eom, Science 306 (2004) 1005.

[10] J.H. Haeni, P. Irvin, W. Chang, R. Uecker, P. Reiche, Y.L. Li, S. Choudhury, W. Tian, M.E. Hawley, B. Craigo, A.K. Tagantsev, X.Q. Pan, S.K. Streiffer, L.Q. Chen, S.W. Kirchoefer, J. Levy, D.G. Schlom, Nature 430 (2004) 758.
[11] Y. Wang, X. Zhou, Q. Chen, B. Chu, Q. Zhang, IEEE Trans. Dielectr. Electr. Insul. 17 (2010) 1036.
[12] X. Hao, Z. Yue, J. Xu, S. An, C.-W. Nan, J. Appl. Phys. 110 (2011) 064109.
[13] A. Chauhan, S. Patel, R. Vaish, C.R. Bowen, Materials 8 (2015) 8009.
[14] M.-H. Cho, D.-H. Ko, Y.G. Choi, K. Jeong, I.W. Lyo, D.Y. Noh, H.J. Kim, C.N. Whang, J. Vac. Sci. Technol. A 191 (2001) 192.
[15] R.B. van Dover, L.F. Schneemeyer, R.M. Fleming, Nature 392 (1998) 162.
[16] M.D. Maeder, D. Damjanovic, N. Setter, J. Electroceram. 13 (2004) 385.
[17] E. Cross, Nature 432 (2004) 24.
[18] W. Li, Huarong Zeng, Kunyu Zhao, Jigong Hao, Jiwei Zhai, Ceram. Int. 40 (2014) 7947.
[19] D. Damjanovic, Rep. Prog. Phys. 61 (1998) 1267.
[20] H. Yu, Z.G. Ye, Appl. Phys. Lett. 93 (2008) 112902.
[21] R. Eitel, C.A. Randall, T.R. Shrout, S.E. Park, Jpn. J. Appl. Phys. 41 (2002) 2099.
[22] K. Maeda, T. Takata, M. Hara, N. Saito, Y. Inoue, H. Kobayashi, K. Domen, J. Am. Chem. Soc. 127 (2005) 8286.
[23] S. Cho, J.-W. Jang, W. Zhang, A. Suwardi, H. Wang, D. Wang, J.L. MacManus-Driscoll, Chem. Mater. 27 (2015) 6635.
[24] L. Chen, W. Ren, W. Zhu, Z.-G. Ye, P. Shi, X. Chen, X. Wu, Xi Yao, Thin Solid Films 518 (2010) 1637.
[25] J.C. Nino, S. Trolier-McKinstry, J. Mater. Res. 19 (2004) 568.
[26] I. Fujii, T. Yamauchi, T. Imai, H. Adachi, T. Wada, Jpn. J. Appl. Phys. 53 (2014) 09PA09.
[27] K. Ueda, H. Tabata, T. Kawai, Appl. Phys. Lett. 75 (1999) 555.
[28] P. Murugavel, J.-H. Lee, J.Y. Jo, H.Y. Sim, J.-S. Chung, Y. Jo, M.-H. Jung, J. Phys.: Condens. Matter 20 (2008) 415208.
[29] S.-H. Yao, J.-K. Yuan, P. Gonon, J. Bai, S. Pairis, A. Sylvestre, J. Appl. Phys. 111 (2012) 104109.
[30] J.L. Maurice, F. Pailloux, A. Barthelemy, O. Durand, D. Imhoff, R. Lyonnet, A. Rocher, J.P. Contour, Philos. Mag. 83 (2003) 3201.
[31] F. Sandiumenge, J. Santiso, L. Balcells, Z. Konstantinovic, J. Roqueta, A. Pomar, J.P. Espinós, B. Martínez, Phys. Rev. Lett. 110 (2013) 107206.
[32] T. Takenaka, H. Nagata, J. Eur. Ceram. Soc. 25 (2005) 2693.
[33] A.F. Devonshire, Adv. Phys. 3 (1954) 85.
[34] M. Itoh, R. Wang, Y. Inaguma, T. Yamaguchi, Y.-J. Shan, T. Nakamura, Phys. Rev. Lett. 82 (1999) 540.
[35] J. Wang, H. Zheng, Z. Ma, S. Prasertchoung, M. Wuttig, R. Droopad, J. Yu, K. Eisenbeiser, R. Ramesh, Appl. Phys. Lett. 85 (2004) 2574.
[36] S.Y. Yang, F. Zavaliche, L. Mohaddes-Ardabili, V. Vaithyanathan, D.G. Schlom, Y.J. Lee, Y.H. Chu, M.P. Cruz, Q. Zhan, T. Zhao, R. Ramesh, Appl. Phys. Lett. 87 (2005) 102903.
[37] S. Bose, S.B. Krupanidhi, Appl. Phys. Lett. 90 (2007) 212902.
[38] C. Michel, J.M. Moreau, G.D. Achenbechi, R. Gerson, W.J. James, Solid State Commun. 7 (1969) 701.
[39] A. Simon, J. Ravez, M. Maglione, J. Phys.: Condens. Matter 16 (2004) 963.
[40] D. Dey, R.C. Bradt, J. Am. Ceram. Soc. 75 (1992) 2529.
[41] Yu.F. Kargin, S.N. Ivicheva, V.V. Volkov, Russ. J. Inorg. Chem. 60 (2015) 619.
[42] S.-H. Baek, C.-B. Eom, Acta Mater. 61 (2013) 2734.
[43] W. Zhang, A. Chen, F. Khatkhatay, C.-F. Tsai, Q. Su, L. Jiao, X. Zhang, H. Wang, ACS Appl. Mater. Interfaces 5 (2013) 3995.
[44] B. Ma, D.K. Kwon, M. Narayanan, U.B. Balachandran, J. Mater. Res. 24 (2009) 2993.
[45] Y. Wang, X. Hao, J. Yang, J. Xu, D. Zhao, J. Appl. Phys. 112 (2012) 034105.
[46] N.D. Zakharov, K.M. Satyalakshmi, G. Koren, D. Hesse, J. Mater. Res. 14 (1999) 4385.
[47] Y.S. Kim, D.H. Kim, J.D. Kim, Y.J. Chang, T.W. Noh, J.H. Kong, K. Char, Y.D. Park, S.D. Bu, J.-G. Yoon, J.-S. Chung, Appl. Phys. Lett. 86 (2005) 102907.
[48] O. Trithaveesak, J. Schubert, C. Buchal, J. Appl. Phys. 98 (2005) 114101.
[49] J. Zhu, L. Zheng, W.B. Luo, Y.R. Li, Y. Zhang, J. Phys. D: Appl. Phys. 39 (2006) 2438.
[50] E.V. Ramana, S.M. Yang, R. Jung, M.H. Jung, B.W. Lee, C.U. Jung, J. Appl. Phys. 113 (2013) 187219.
[51] M. Kuwabara, K. Goda, K. Oshima, Phys. Rev. B. 42 (1990) 10012.
[52] E.P. Smirnova, A.V. Sotnikov, N.V. Zaitseva, H. Schmidt, M. Weihnacht, Phys. Solid State 56 (2014) 996.
[53] S. Kumaragurubaran, T. Nagata, K. Takahashi, S.-G. Ri, Y. Tsunekawa, S. Suzuki, T. Chikyow, Jpn. J. Appl. Phys. 54 (2015) 04DH02.
[54] C.B. Eom, R.B. Van Dover, Julia M. Phillips, D.J. Werder, J.H. Marshall, C.H. Chen, R.J. Cava, R.M. Fleming, D.K. Fork, Appl. Phys. Lett. 63 (1993) 2570.
[55] H. Nonomura, H. Fujisawa, M. Shimizu, H. Niu, Jpn. J. Appl. Phys. 41 (2002) 6682.
[56] Y.K. Wang, T.Y. Tseng, P. Lin, Appl. Phys. Lett. 80 (2002) 3790.
[57] D. Bao, S.K. Lee, X. Zhu, M. Alexe, D. Hesse, Appl. Phys. Lett. 86 (2005) 082906.
[58] O. Lee, S.A. Harrington, A. Kursumovic, E. Defay, H. Wang, Z. Bi, C.-F. Tsai, L. Yan, Q.X. Jia, J.L. MacManus-Driscoll, Nano Lett. 12 (2012) 4311.
[59] Y.H. Chu, L.W. Martin, Q. Zhan, P.L. Yang, M.P. Cruz, K. Lee, M. Barry, S.Y. Yang, R. Ramesh, Ferroelectrics 354 (2007) 167.
[60] G.W. Pabst, L.W. Martin, Y.-H. Chu, R. Ramesh, Appl. Phys. Lett. 90 (2007) 072902.
[61] D.S. Rana, K. Takahashi, K.R. Mavani, I. Kawayama, H. Murakami, M. Tonouchi, T. Yanagida, H. Tanaka, T. Kawai, Phys. Rev. B 75 (2007) 060405(R).
[62] D.S. Rana, K. Takahashi, K.R. Mavani, I. Kawayama, H. Murakami, M. Tonouchi, Phys. Rev. B 77 (2008) 024105.
[63] V. Moshnyaga, B. Damaschke, O. Shapoval, A. Belenchuk, J. Faupel, O.I. Lebedev, J. Verbeeck, G. van Tendeloo, M. Mucksch, V. Tsurkan, R. Tidecks, K. Samwer, Nat. Mater. 2 (2003) 247.
[64] H. Zheng, J. Wang, S.E. Lofland, Z. Ma, L. Mohaddes-Ardabili, T. Zhao, L. Salamanca-Riba, S.R. Shinde, S.B. Ogale, F. Bai, D. Viehland, Y. Jia, D.G. Schlom, M. Wuttig, A. Roytburd, R. Ramesh, Science 303 (2004) 661.
[65] J.L. MacManus-Driscoll, S.R. Foltyn, Q.X. Jia, H. Wang, A. Serquis, L. Civale, B. Maiorov, M.E. Hawley, M.P. Maley, D.E. Peterson, Nat. Mater. 3 (2004) 439.
[66] E.-M. Choi, A. Kursumovic, O.J. Lee, J.E. Kleibeuker, A. Chen, W. Zhang, H. Wang, J.L. MacManus-Driscoll, ACS Appl. Mater. Interfaces 6 (2014) 14836.
[67] M. Lorenz, V. Lazenka, P. Schwinkendorf, F. Bern, M. Ziese, H. Modarresi, A. Volodin, M.J. Van Bael, K. Temst, A. Vantomme, Marius Grundmann, J. Phys. D: Appl. Phys. 47 (2014) 135303.
[68] J. Wu, J. Wang, J. Appl. Phys. 106 (2009) 104111.
[69] M. Bousquet, J.-R. Duclère, B. Gautier, A. Boulle, A. Wu, S. Députier, D. Fasquelle, F. Rémondière, D. Albertini, C. Champeaux, P. Marchet, M. Guilloux-Viry, P. Vilarinho, J. Appl. Phys. 111 (2012) 104106.
[70] Y. Ahn, J. Seo, K. Jo Lee, J.Y. Son, J. Cryst. Growth 437 (2016) 10.
[71] S. Cho, C. Yun, S. Tappertzhofen, A. Kursumovic, S. Lee, P. Lu, Q.X. Jia, M. Fan, J. Jian, H. Wang, S. Hofmann, J.L. MacManus-Driscoll, Nat. Commun. 7 (2016) 12373.
[72] B. Chu, X. Zhou, K. Ren, B. Neese, M. Lin, Q. Wang, F. Bauer, Q.M. Zhang, Science 313 (2006) 334.
[73] S. Kwon, W. Hackenberger, E. Alberta, E. Furman, M. Lanagan, IEEE Electr. Insul. Mag. 27 (2011) 43.
[74] K. Yao, S. Chen, M. Rahimabady, M.S. Mirshekarloo, S. Yu, F.E.H. Tay, T. Sritharan, L. Lu, IEEE Trans. Ultrason. Ferroelectr. Freq. Control 58 (2011) 1968.
[75] T.M. Correia, M. McMillen, M.K. Rokosz, P.M. Weaver, J.M. Gregg, G. Viola, M.G. Cain, J. Am. Ceram. Soc. 96 (2013) 2699.
[76] B. Peng, Q. Zhang, X. Li, T. Sun, H. Fan, S. Ke, M. Ye, Y. Wang, W. Lu, H. Niu, J.F. Scott, X. Zeng, H. Huang, Adv. Electron. Mater. 1 (2015) 1500052.
[77] J. Parui, S.B. Krupanidhi, Appl. Phys. Lett. 92 (2008) 192901.
[78] H. Ogihara, C.A. Randall, S. Trolier-McKinstry, J. Am. Ceram. Soc. 92 (2009) 1719.
[79] B. Ma, M. Narayanan, U.B. Balachandran, Mater. Lett. 63 (2009) 1353.
[80] H. Pan, Y. Zeng, Y. Shen, Y.-H. Lin, J. Ma, L. Li, C.-W. Nan, J. Mater. Chem. A 5 (2017) 5920.
[81] X. Hao, J. Zhai, Xi Yao, J. Am. Ceram. Soc. 92 (2009) 1133.
[82] X. Hao, J. Zhou, S. An, J. Am. Ceram. Soc. 94 (2011) 1647.
[83] M. Ye, Q. Sun, X. Chen, Z. Jiang, F. Wang, J. Am. Ceram. Soc. 94 (2011) 3234.
[84] N. Ortega, A. Kumar, J.F. Scott, D.B. Chrisey, M. Tomazawa, S. Kumari, D.G.B. Diestra, R.S. Katiyar, J. Phys.: Condens. Matter 24 (2012) 445901.

Seungho Cho is an Assistant Professor in the School of Materials Science and Engineering at Ulsan National Institute of Science and Technology (UNIST). He completed his Ph.D. degree from Chemical Engineering, Pohang University of Science and Technology (POSTECH) and worked as postdoctoral research associates in the Department of Chemistry at POSTECH and Department of Materials Science and Metallurgy at University of Cambridge. His research is in the area of crystal growth and applications of metal oxide powders and films.

Chao Yun is a Ph.D. candidate studying in the Driscoll Group, Department of Materials Science and Metallurgy, University of Cambridge. He received his Master's and Bachelor's degree in Peking University and Lanzhou University, China in 2014 and 2011, respectively. His research focuses on magnetoelectric properties in self-assembled vertical heteroepitaxy nanocomposites.

Yoon Seo Kim is a graduate student studying in the School of Materials Science and Engineering at Ulsan National Institute of Science and Technology (UNIST). Her research interests are mainly on metal oxide crystal growth and applications.

Han Wang is a Ph.D. candidate in the School of Materials Engineering at Purdue University. She received the B.E. in materials engineering from Nanchang University, China, and M.E. in materials engineering from Stevens Institute of Technology, NJ. Her major interests are strain-engineered bismuth-based oxide thin films for multifunction and microcharacterization of flash sintering.

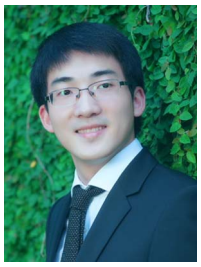

Jie Jian received his B.S. degree in 2010 from Zhejiang University, Hangzhou, China, and Ph.D. degree in Electrical Engineering from Texas A&M University, College Station, USA in 2016. His research mainly lies in nano-structured functional oxide and nitride materials. The interest focuses on electrical properties, magnetic properties, phase transformation properties, optical properties etc.

Wenrui Zhang received his Ph.D. in Materials Science and Engineering from Texas A&M University in 2015. Currently, he is a research associate at Center for Functional Nanomaterials, Brookhaven National Laboratory. His research focuses on functional thin film heterostructures of semiconductors and strongly correlated materials for energy, electronics and magnetism.

Jijie Huang received his Bachelor's degree from Wuhan University of Technology in 2009, Master's degree from Zhejiang University in 2012, and Ph.D. from Texas A&M University in 2016. Now he is a postdoctoral research associate in Prof. Haiyan Wang's group at Purdue University. His research interests are mainly on functional thin film growth and characterization.

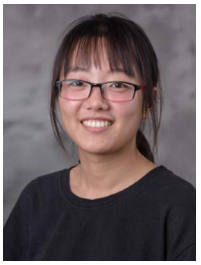

Xuejing Wang is a Ph.D. candidate in the group guided by Prof. Haiyan Wang at the Department of Materials Engineering, Purdue University. She received her B.E in the Materials Engineering from Central South University, China, and M.S. from SUNY Stony Brook University, USA. Her current research interest includes functional nanocomposite thin film design for tunable optical properties and applications.

Haiyan Wang is the Turner Chair Professor of Engineering with a joint appointment in the Schools of Materials Engineering and the School of Electrical and Computer Engineering at Purdue University since 2016. She received her Ph.D. degree from North Carolina State University and conducted her postdoc research at Los Alamos National Laboratory during 2013–2015. She was on the faculty at Texas A&M University from 2006 to 2016. She has published over 400 journal articles in the areas of ceramic thin films, nanocomposites, functional ceramics, TEM and in-situ TEM. She is the fellow of ACerS, APS, AAAS and ASM.

Judith L. MacManus-Driscoll is a Professor in the Materials Science Department at the University of Cambridge. She is also a visiting staff member at Los Alamos National Laboratory. Her research is in the area of electronic oxide thin films, i.e., superconductors, ferroelectrics, multiferroics, magnetics and semiconductors. She is a Fellow many learned societies around the world.